Influence of structural transition on transport and optical properties of Ni 2 MnGa alloy

Y. Zhou, Xuesong Jin, Huibin Xu, Y. V. Kudryavtsev, Y. P. Lee, and J. Y. Rhee

Citation: Journal of Applied Physics **91**, 9894 (2002); doi: 10.1063/1.1478131
View online: http://dx.doi.org/10.1063/1.1478131
View Table of Contents: http://scitation.aip.org/content/aip/journal/jap/91/12?ver=pdfcov
Published by the AIP Publishing

Influence of structural transition on transport and optical properties of Ni_2MnGa alloy

Y. Zhou, Xuesong Jin, and Huibin Xu
Department of Material Science and Engineering, Beijing University of Aeronautics and Astronautics, Beijing 100-083, People's Republic of China

Y. V. Kudryavtsev and Y. P. Lee[a)]
Department of Physics, Hanyang University, Seoul 133-791, Korea

J. Y. Rhee
Department of Physics, Hoseo University, Asan 336-795, Korea

(Received 6 August 2001; accepted for publication 26 March 2002)

The transport and optical properties of Ni_2MnGa alloy in the martensitic and austenitic states were investigated. The dependence of the temperature coefficient of resistivity on temperature shows kinks at the structural and ferroparamagnetic transitions. Electron-magnon and electron-phonon scattering are analyzed to be the dominant scattering mechanisms of the Ni_2MnGa alloy in the martensitic and austenitic states, respectively. It was observed that the martensite reveals a higher Debye temperature compared to the austenite, which was explained by a difference in the restoring coefficient between atoms. A Lorentz model that consists of two oscillators was employed to fit the interband contribution to optical conductivity (OC). It is found that the structural transition plays a more important role for the changes in OC spectrum than the thermal-expansion effect. © *2002 American Institute of Physics.* [DOI: 10.1063/1.1478131]

I. INTRODUCTION

Reversible structural deformations attract much interest in view of the development of materials for engineering applications such as robotics. Such a deformation with a strain up to 20% is present in shape-memory alloys.[1] While the shape-memory effect in most of the current commercial actuator materials like TiNi is related to a martensitic phase transformation driven by temperature, the magnetic control of such a transformation would be faster and more efficient. For this purpose, some magnetically driven actuator materials, such as ternary and intermetallic Heusler alloys with a composition X_2YM, are being developed. A prototypical example is Ni_2MnGa.[2] Several studies have shown the magnetic properties and structures of this alloy by means of x-ray and neutron diffraction measurements.[3,4] It was found that the alloy has an ordered $L2_1$ structure with primarily ferromagnetic ordering. In addition, investigations on the structural phase transformation and deformation of the $L2_1$ structure in the ferromagnetic Ni_2MnGa Heusler alloy have been carried out.[5–13] A premartensitic transition was also identified in the alloy.[10,13]

Resistivity measurement has been employed to investigate the structural and magnetic transitions of Ni_2MnGa alloy because of its simplicity and efficiency. Vasil'ev *et al.* observed a clear jump at the martensitic transition and a slope change at the ferroparamagnetic transition from the resistivity measurement of $Ni_{2-x}Mn_{1+x}Ga$ alloys.[14] For $Ni_{2+x}Mn_{1-x}Ga$ alloys, the resistivity shows an evident kink at the martensitic transition and a discontinuous slope change at the premartensitic transition. The characteristic temperatures coincided well with the previous direct structural results in other studies.[15] The optical properties of Heusler alloys have also been widely investigated. It was found that PtMnSb alloy exhibits a very large Kerr rotation and half-metallic ferromagnetic properties.[16,17] The optical properties of X_2MnSn (X=Ni,Pd) Heusler alloys were reported by Kirillova *et al.*[18] They observed that the main absorption band experiences no dramatic change upon transition through the Curie temperature. The most pronounced changes upon transition to the paramagnetic state are observed for $T/T_c \geqslant 1.4$ in Ni_2MnSn and for $T/T_c \geqslant 2.38$ in Pd_2MnSn. This means that, although the macroscopic magnetization vanishes above T_c, the general structure of the energy bands and their exchange splitting remain almost unchanged. A rearrangement of the electronic band structure due to a destruction of the magnetic order occurs at a temperature far above the Curie temperature.

However, the optical and transport properties, and the electronic structure of Ni_2MnGa alloy are not well understood. The effect of the structural transition on the optical and transport properties of alloy has not been investigated yet. In this work, we study the optical and transport properties of the Ni_2MnGa Heusler alloy at low and room temperature (RT), i.e., in the ferromagnetic martensitic and the austenitic state, respectively. The purpose of this article is to elucidate experimentally the influence of the structural transition on the transport and optical properties.

II. EXPERIMENT AND SIMULATION DETAILS

The stoichiometric Ni_2MnGa alloy was prepared by melting high-purity (99.99 wt %) Ni, Mn, and Ga pieces in

a)Electronic mail: yplee@hanyang.ac.kr

an arc furnace with a water-cooled Cu hearth. Subsequent homogenization of the ingot was achieved by a vacuum annealing at 1273 K for 5 h. In order to measure the transport and optical properties, samples of various shapes were spark cut from the homogenized ingot. The resistivity measurement was done in a temperature range from 4.2 to 400 K by using a four-probe method.

X-ray fluorescence analysis revealed that the composition of prepared samples is nearly stoichiometric. X-ray diffraction was also carried out to verify the structural phase. A comparison between the computer simulated (for the perfect cubic structure) and the experimental patterns showed that the samples are predominantly in the cubic phase, even though there are a few additional but minor experimental diffraction lines probably, resulting from negligible impurity phases.

Specimens for the optical measurements were mechanically polished and annealed at 770 K for 150 min in a vacuum of 5×10^{-6} Torr, and then electrolitically polished in a solution of alcohol with 50 vol % nitric acid. The current density was 10 mA/cm^2. The optical and magneto-optical measurements were carried out in a vacuum of 5×10^{-6} Torr. Prior to the measurements, the specimen was sputtered by an Ar-ion beam to remove the superficial oxide layer and absorbed gases on the surface.

The optical properties (the real and imaginary parts of the complex refractive index, $N=n-ik$) were measured at RT in a spectral range of 0.5–4.5 eV at a fixed incidence angle of 73° by using the spectroscopic ellipsometry technique. The obtained values of n and k were used in calculating the spectral dependencies of not only the real (ε_1) and imaginary (ε_2) parts of the diagonal components of the dielectric function ($\varepsilon_{xx}=\varepsilon_{yy}=\varepsilon_{zz}=\varepsilon=\varepsilon_1-i\varepsilon_2$), but also the optical conductivity (OC, σ), by using expressions: $\varepsilon_1=n^2-k^2$ and $\varepsilon_2=2nk$, and $\sigma(\hbar\omega)=\varepsilon_2\omega/4\pi$ where ω is the angular frequency of light.

A phenomenological Lorentz-oscillator (LO) model was used to fit the interband contribution to the OC. The LO model is given by[19]

$$\sigma=\frac{\omega}{4\pi}\frac{EA_jB_j}{(E_j^2-E^2)^2+E^2B_j^2},$$

where $A_j=4\pi ne^2h/m_j^*$, $B_j=h/\tau_j$, and $E=\hbar\omega$. E_j is the center energy of oscillator j, which could potentially correspond to one of the critical transitions of the material. Each oscillator might be due to an integrated combination of transitions from different parts of the band structure. m_j^* is the effective mass of oscillator j and τ_j the relaxation time. e is the electron charge, h Planck constant, and n the carrier density of the material. A_j and B_j are defined as the amplitude and the broadening factor, respectively, of oscillator j. A_j, B_j, and E_j are the fitting parameters in the regression. When E_j is zero, the corresponding oscillator has the same form as the classical Drude model for free carriers.

III. RESULTS AND DISCUSSION

The temperature dependence of resistance and temperature coefficient of resistivity (TCR) of Ni_2MnGa alloy is shown in Fig. 1. The dc resistivity measurements provide a simple and effective way to detect both structural and magnetic transitions. As revealed in Fig. 1, the resistance shows a metallic behavior. On the other hand, the TCR reveals an abrupt change at a temperature T_S (220 K) and steeply decreases to zero as temperature passes through T_C (380 K). Since the resistivity reflects the crystal lattice deformation, a sharp kink in TCR curve is consistently connected with a critical temperature at which the structural transition occurs. A martensite–austenite transition from tetragonal to cubic $L2_1$ structure was observed at 220 K for Ni_2MnGa alloy,[20] and T_S of the present work coincides with the reported structural transition temperature. T_C in Fig. 1 indicates the ferro-paramagnetic transition temperature. The decrease of TCR during the transition can be attributed to the disappearance of electron scattering on magnetic fluctuations.[14]

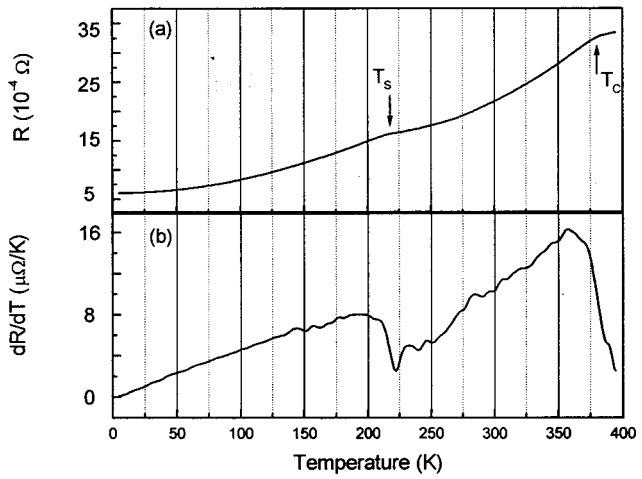

FIG. 1. Temperature dependence of (a) resistance and (b) temperature coefficient of resistivity of Ni_2MnGa alloy.

The usual expression for the temperature dependence of resistivity for metals and alloys can be described by the Matthiessen rule $\rho(T)=\rho_0+\rho_i(T)$, where ρ_0 is the temperature independent residual resistivity (mainly due to electron defect scattering without absorption or emission of phonons) and $\rho_i(T)$ is the so-called ideal resistivity provided by inelastic electron scattering. The ideal resistivity includes the electron-phonon, electron-electron and electron-magnon (for magnetic materials) scatterings. Each mechanism gives rise to a different power law T^α for the temperature dependence of resistivity.

It was shown by Ptitsina *et al.* that the electron–phonon interaction is conducted mainly by two processes: the first is the so-called pure electron-phonon scattering and the second is the inelastic scattering from vibrating impurities. The temperature dependence of the electron-phonon scattering can be written as similar to the Bloch–Grüneisen law:[21]

$$\rho_{B-G}=\frac{1}{2}\rho_0\frac{\pi\beta_l\tau}{\hbar(p_F\mu_l)^4}(k_BT)^5\int_0^{\Theta_D/T}\frac{x^5dx}{(e^x-1)(1-e^{-x})}. \quad (1)$$

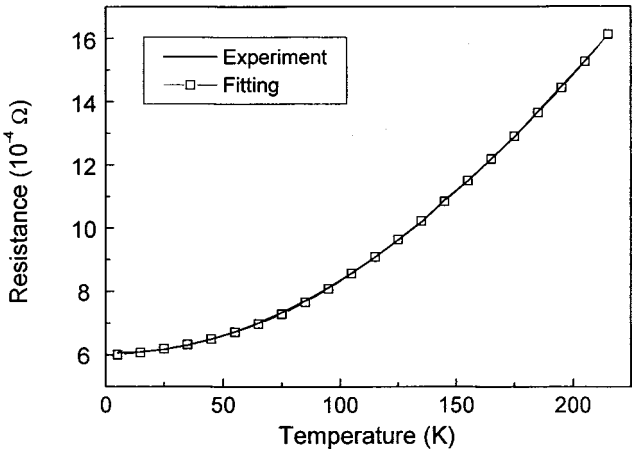

FIG. 2. Experimental and fitted temperature dependence of the resistance of Ni_2MnGa alloy in the martensitic state.

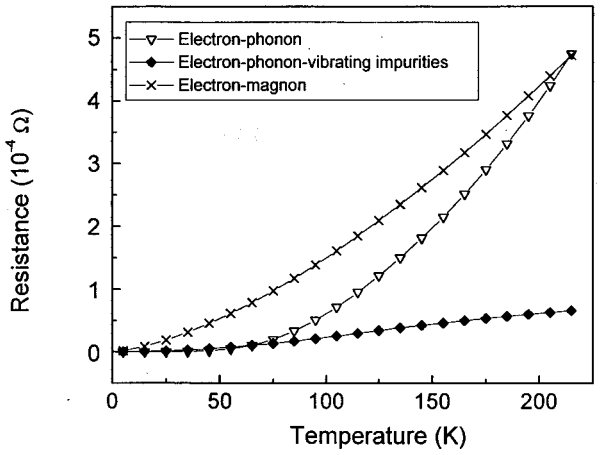

FIG. 3. Contributions of different scattering mechanisms to the resistance of Ni_2MnGa alloy in the martensitic state.

The temperature dependence of resistivity caused by scattering based on the electron-phonon-vibrating impurities is expressed by[22]

$$\rho_{VIS}=\rho_0\left[2\left(\frac{\mu_l}{\mu_t}\right)\beta_t-\left(1-\frac{\pi^2}{16}\right)\beta_l\right]\frac{4\pi^2k_B^2}{3E_Fp_F\mu_l}T^2 \times\int_0^{\Theta_D/T}\frac{e^x(x-1)+1}{(e^x-1)^2}xdx, \quad (2)$$

where $\tau=l/\upsilon_F$ is the elastic transport time. μ_l and μ_t are the sound velocity of the longitudinal and transverse phonons, β_l and β_t are constants of electron coupling with the longitudinal and transverse phonons, and E_F and p_F are the Fermi energy and momentum, respectively. Θ_D is the Debye temperature. It is noted from Eqs. (1) and (2) that at low temperatures the resistivity is proportional to T^5 for the pure electron-phonon scattering and to T^2 for the case of electron scattering by the vibrating impurities. Electron-magnon scattering gives rise to a temperature exponent of $\alpha=3/2$ in dilute ferromagnetic alloys.[23]

In order to carry out analyses of the experimental data, the following function was employed:

$$R=A+BT^5F_1(T)+CT^2F_2(T)+DT^{3/2},$$

where A is the residual resistance, B, C, and D are fitting constants:

$$F_1(T)=\int_0^{\Theta_D/T}\frac{x^5dx}{(e^x-1)(1-e^{-x})},$$

and

$$F_2(T)=\int_0^{\Theta_D/T}\frac{e^x(x-1)+1}{(e^x-1)^2}xdx.$$

There are five parameters in this fitting procedure: A, B, C, D, and Θ_D in function F_1 and F_2. Figure 2 presents the temperature dependence of the experimental and fitted resistance for the martensitic state. The resultant values for the fitting parameters are given in Table I. The fitting shows an excellent coincidence with the experiment. The different scattering mechanisms for the resistance are shown in Fig. 3. The electron-magnon scattering is dominant for a temperature lower than 75 K. The contributions of electron-magnon and electron-phonon scatterings increase with temperature. When the temperature reaches about 220 K, these two kinds of mechanisms give almost the same contributions to the resistance. On the other hand, the electron-phonon-vibrating impurities scattering is relatively weak, slowly increasing with temperature. Thus, the electron-magnon scattering is the dominant mechanism in the martensite at low temperatures, while in a high temperature range the electron-magnon and electron-phonon scatterings play a combined role for the resistance of alloy.

Figure 4 is the experimental and fitted resistance of Ni_2MnGa alloy in the austenite state. The results also agree well with each other. The contributions of relevant scattering mechanisms are shown in Fig. 5. In the whole temperature range, the electron-phonon scattering gives the greatest significance. The magnitudes of the electron-phonon-vibrating impurities and electron-magnon scatterings are smaller than that of the main electron-phonon scattering by an order of one and three, respectively. It is thought that the governing role of the electron-phonon scattering results from significant vibration of the lattice at high temperatures.

It is also found that Debye temperature of the martensite

TABLE I. Fitting parameters to the $R(T)$ data for two structural states of Ni_2MnGa alloy.

Structural state	A (Ω)	B (K^{-5})	C (K^{-2})	D ($K^{-1.5}$)	Θ_D (K)
Martensite	0.00060	6.61×10^{-17}	6.67×10^{-9}	1.17×10^{-7}	624.6
Austenite	0.00081	8.08×10^{-16}	6.08×10^{-12}	6.52×10^{-10}	296.1

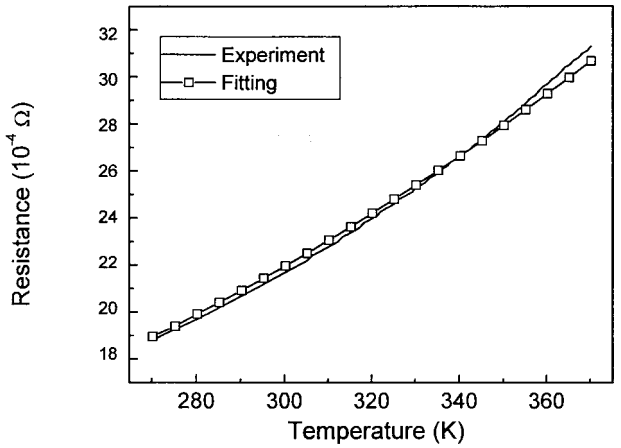

FIG. 4. Experimental and fitted temperature dependence of the resistance of Ni_2MnGa alloy in the austenitic state.

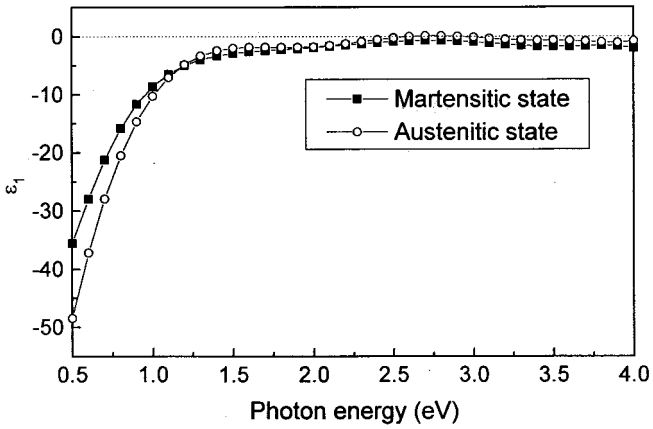

FIG. 6. Experimental spectra of the real part of the diagonal component of the dielectric function for Ni_2MnGa alloy in the martensitic and austenitic states.

is higher with respect to the austenite (Table I). The Debye temperature is defined by

$$\Theta_D = \frac{\hbar}{k_B}\left(\frac{12N\pi^2}{V}\right)^{1/3} C, \tag{3}$$

where N is the atomic number, V is the volume, and

$$C = a\sqrt{\beta/m}$$

is the wave velocity. Again, a is the lattice constant, β is the restoring coefficient between atoms, and m is the atomic mass. Thus, Eq. (3) could be rewritten as

$$\Theta_D = a\frac{\hbar}{k_B}\left(\frac{12N\pi^2}{V}\right)^{1/3}\sqrt{\frac{\beta}{m}}.$$

Since the parameters except β do not change appreciably upon the structural transition, β becomes the dominant factor whose enhancement leads to an increase in Θ_D for the martensitic state. This can also be supported by evaluating the elastic modulus of Ni_2MnGa alloys during the structural transition. Chernenko *et al.* observed a higher elastic modulus for the martensite than the austenite,[24] which means a stronger interaction between atoms, that is, a larger restoring coefficient.

Figure 6 is the experimental spectra of the real part of the diagonal component of the dielectric function for the martensitic and austenitic Ni_2MnGa alloy. Both ε_1 spectra are negative, and increase in absolute value with decreasing photon energy in the low-energy range. The experimental ε_1 spectrum of the austenitic state intersects the zero line twice at 2.6 and 2.9 eV, reaching its maximum at 2.8 eV. This indicates a significant contribution to the optical absorption from free carriers. It is well known that, in metals, the negative value of ε_1 in the low-energy region is caused by the acceleration mechanism of free electrons, while the positive contribution to ε_1 is usually concerned with the interband transition of bound electrons.[25]

The OC spectra for Ni_2MnGa alloy are shown in Fig. 7. It can be seen that both OC spectra reveal similar shapes and clearly manifest absorption peaks at about 1.8 and 3.2 eV. In metal, the OC spectrum consists of contributions from both

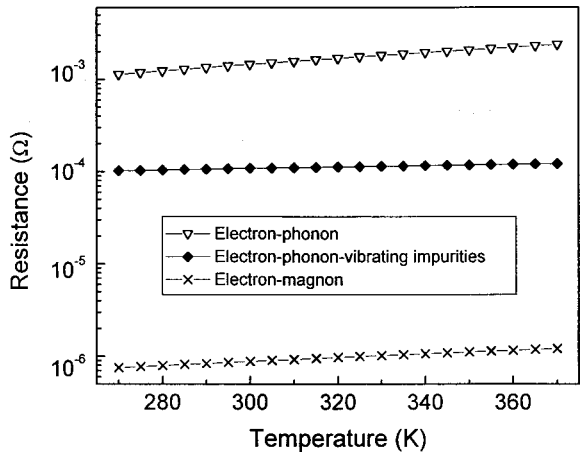

FIG. 5. Contributions of different scattering mechanisms to the resistance of Ni_2MnGa alloy in the austenitic state.

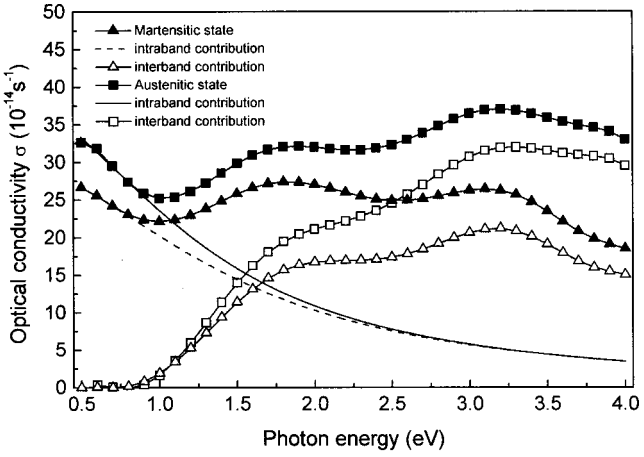

FIG. 7. Optical conductivity spectra for Ni_2MnGa alloy in the martensitic and austenitic states. The contributions from intraband and interband transitions are also drawn.

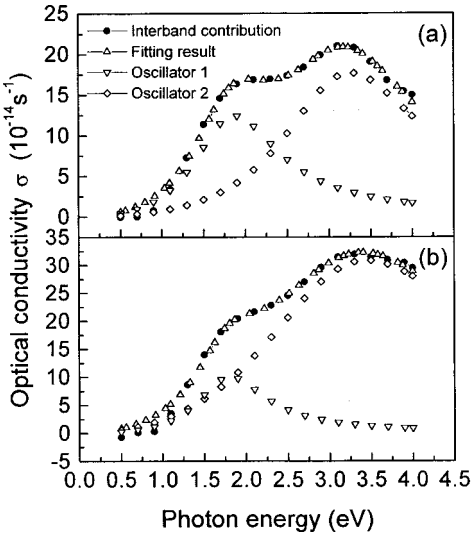

FIG. 8. Experimental and fitted interband contributions to the optical conductivity spectra for Ni_2MnGa alloy in the (a) martensitic and (b) austenitic states. The contribution of each oscillator is drawn together.

intraband and interband transitions. In order to separate these, the part from intraband transitions (σ_{intra}) was fitted by using the following equation:[19]

$$\sigma_{\text{intra}}=\frac{\Omega^2\gamma}{4\pi(\omega^2+\gamma^2)},$$

where Ω is the plasma frequency and γ is the relaxation frequency. The interband contribution (σ_{inter}) is obtained as the subtraction of σ_{intra} from the experimental spectrum. σ_{intra} and σ_{inter} of Ni_2MnGa alloy are plotted in Fig. 7. The fitting coefficients Ω^2 and γ of σ_{intra} are 6.57×10^{30} s^{-2} and 22×10^{14} s^{-1}, and 7.35×10^{30} s^{-2} and 19×10^{14} s^{-1} for the austenitic and martensitic states, respectively.

The LO model is applied to analyze σ_{inter}. The results are presented in Fig. 8 and the values for the fitting parameters are given in Table II. In the fitting process, two oscillators were employed to achieve the best coincidence with the experiment. In other words, more or fewer oscillators led to a worse agreement. Furthermore, all the correlation coefficients between floating oscillator parameters were acceptably low in case of two oscillators (a high correlation indicates lack of uniqueness). The degree of uncertainty for each parameter, provided by the regression procedure, are listed in Table II. Note that the uncertainty for the center energy is low for both oscillators, while that for the amplitude is relatively high. It is also found in Table II that the oscillator parameters are changed in value upon the martensite–austenite transition, which results from the thermal expansion and the structural transition. In case of thermal expansion, the absorption peaks are broadened and their intensities decrease. According to our results (Fig. 8 and Table II), the broadening factor of oscillator 1 is reduced, that is, the peak becomes narrower by the martensite–austenite transition and the amplitude of oscillator 2 is drastically increased. This means that the structural transition plays a more important role for the changes in OC spectrum compared to the thermal-expansion effect. Ni_2MnGa alloy have a cubic lattice with $a=5.822$ Å in the austenitic state, on the other hand, a tetragonal structure with $a=b=5.90$ and $c=5.44$ Å in the martensitic state. It is thought that the structural transformation, causes the lattice deformation and again the changes in electronic band structure.

TABLE II. Lorentz-oscillator fitting parameters for the interband contributions to the optical conductivity of Ni_2MnGa alloy in two different states.

No.	Oscillators	Martensitic state	Austenitic state
1	A^a (eV)	12.9 ± 0.67	8.29 ± 0.30
	B^b (eV)	1.25 ± 0.06	1.00 ± 0.06
	E^c (eV)	1.87 ± 0.03	1.80 ± 0.03
2	A^a (eV)	30.1 ± 0.67	81.9 ± 0.61
	B^b (eV)	2.06 ± 0.06	3.21 ± 0.33
	E^c (eV)	3.26 ± 0.03	3.44 ± 0.09

[a]Amplitude of oscillator.
[b]Broadening factor of oscillator.
[c]Center energy of oscillator.

IV. CONCLUSIONS

The transport and optical properties of Ni_2MnGa alloy were measured for the martensitic and austenitic states. The temperature dependence of TCR shows kinks at the structural and ferroparamagnetic transitions. It was elucidated that the electron-magnon and electron-phonon scatterings are the main contributions to the resistivity of Ni_2MnGa alloy in the martensitic and austenitic states, respectively. The Debye temperatures of both martensite and austenite were also estimated; a higher Debye temperature for the martensitic state was observed, which is connected with a larger restoring coefficient between atoms. A Lorentz model based on two oscillators was employed to fit the interband contribution to the OC. It was found that the structural transition plays a more important role for the changes in the OC spectrum than the thermal-expansion effect. Additional investigation on the magneto-optical properties and the electronic structure of Ni_2MnGa Heusler alloy, in connection with phase transformation and the ferroparamagnetic transition, are also underway.

ACKNOWLEDGMENTS

This work was supported by a Korea Research Foundation Grant No. KRF-2001-015-DS0015. This work was also supported by NSFC.

[1] C. M. Wayman, MRS Bull. **13**, 49 (1993).
[2] K. Ullakko, J. K. Huang, C. Kantner, R. C. O'Handley, and V. V. Kokorin, Appl. Phys. Lett. **69**, 1966 (1996).
[3] A. Zheludev, S. M. Shapiro, P. Wochner, A. Schwartz, M. Wall, and L. E. Tanner, Phys. Rev. B **51**, 11310 (1995).
[4] T. E. Stenger and J. Trivisonno, Phys. Rev. B **57**, 2735 (1998).
[5] A. Planes, E. Obrado, A. Gonzalez-Comas, and L. Manosa, Phys. Rev. Lett. **79**, 3926 (1997).
[6] V. V. Kokorin, V. A. Chernenko, E. Cesari, J. Pons, and C. Segui, J. Phys.: Condens. Matter **8**, 6457 (1996).
[7] A. Zheludev, S. M. Shapiro, P. Wochner, and L. E. Tanner, Phys. Rev. B **54**, 15045 (1996).
[8] V. A. Chernenko, C. Segui, E. Cesari, J. Pons, and V. V. Kokorin, Phys. Rev. B **57**, 2659 (1998).
[9] F. Zuo, V. Su, and K. H. Wu, Phys. Rev. B **58**, 11127 (1998).

[10] J. Y. Rhee, J. Korean Phys. Soc. **34**, 191 (1999).
[11] V. V. Martynov, J. Phys. IV **5**, C891 (1995).
[12] K. Ooiwa, K. Endo, and A. Shinogi, J. Magn. Magn. Mater. **104–107**, 2011 (1992).
[13] P. J. Webster, K. R. A. Ziebeck, S. L. Town, and M. S. Peak, Philos. Mag. **49**, 295 (1984).
[14] A. Vasil'ev *et al.*, Phys. Rev. B **59**, 1113 (1999).
[15] F. Zuo *et al.*, J. Phys.: Condens. Matter **11**, 2821 (1999).
[16] P. G. van Engen, K. H. Buschow, R. Jongebreur, and M. Erman, Appl. Phys. Lett. **42**, 202 (1983).
[17] R. A. de Groot, F. M. Mueller, P. G. van Engen, and K. H. J. Buschow, Phys. Rev. Lett. **50**, 2024 (1983).
[18] M. M. Kirillova, Yu. I. Kuz'min, Yu. V. Knyazev, and E. I. Shreder, Phys. Met. Metallogr. **83**, 590 (1997).
[19] R. W. Collins and K. Vedam, *Optical Properties of Solids* (VCH, Weinheim, 1995).
[20] C. H. Yu *et al.*, J. Appl. Phys. **87**, 6292 (2000).
[21] B. L. Altshuler, Zh. Eksp. Teor. Fiz. **75**, 1330 (1978).
[22] M. Yu. Reizer and A. V. Sergeev, Zh. Eksp. Teor. Fiz. **92**, 2291 (1987).
[23] S. Chakraborty and A. K. Majumdar, Phys. Rev. B **53**, 6235 (1996).
[24] V. Chernenko *et al.*, Mater. Sci. Forum **327–328**, 485 (2000).
[25] M. M. Noskov, *Optical and Magneto-Optical Properties of Metals* (UNTS, Sverdlovsk, 1983).